

Investigating the Effect of Cooling Air Passage on the Temperature Distribution in Turbine Blades

Abbas sahi shareef - Wasit University / College of Engineering^o

الخلاصة:-

يَهْتَم هذا البحث بدراسة تأثير نسبة السرعة على توزيع درجات الحرارة بين ريش التورباين. أن التحقيق العملي و النظري يُقَدِّم وسيلة مفيدة للحصول على معلومات نوعية لمنطقة الاحتراق وكيفية تأثير التيار الرئيسي بتياراة النفث و التي تعمل على تغير توزيع درجات الحرارة. • يمكن الرجوع الى الجزء الخاص بمنظومة الاختبار لملاحظة خطوات التعيير والقوانين الخاصة بجهاز مسبار الفتحات الخمسة، مسبار الضغط الأستاتيكي • لقد دُرست عدّة حالات في البحث بإستعمال ثلاثة نسبة للسرعة $V_R=0.5$ (1 and 2)، وثلاثة مواقع لتيارات النفث (from the end wall) (75% ,90% and 99%) و بزوايا نفث $(\theta=45^0)$ وقطر فتحات النفث تساوي $(d=0.1 \text{ cm})$. حيث تم بناء برنامج حاسوبي يعمل بطريقة (finite volume) ،[SIMPLE]. أن الحسابات بينت أن اعلا درجة حرارة تحدث عندما يكون نسبة السرعة $V_R=0.5$ وموقع تيار النفث هو (99% from the end wall) ، وأن التغير في درجات يكون أعلا ما يمكن عند منطقة النفث ويقل باتجاه المناطق البعيدة عن منطقة النفث وأن درجة الحرارة تزداد مع نقصان نسبة السرعة عند ثبوت منطقة النفث

Abstract

This paper was carried out to study the effect of the velocity ratio of cooling air on the temperature distribution in the turbine blade passage. The experimental and computation method gives a clear picture of the penetration area and the temperature distribution in the passage. All the calibration of the instrument and the laws of the five hole probe may be notes in the section test rig. Several cases have been studied in this research by using three-velocity ratio ($V_R=0.5$, 1 and 2), and three different locations (99% ,90% and 75%) from the end wall with the jets angle $\theta=45^0$.the hole diameter $(d=0.1 \text{ cm})$. The procedure solves the governing equation numerically by using the finite volume method semi implicit method for pressure-linked equation. Therefore the present results show an accepted agreement if compared with experimental work. The maximum temperature occurred of $V_R=0.5$ and the jet location (99%) from the end wall .Therefore the temperatures are fluctuated at the core, and decreased gradually from the jet core to outside. The temperatures are increase with decrease the velocity ratio at the same the jut location from the axial chored.

Introduction:

An increase in the thrust and cycle efficiency of gas turbines can be achieved through higher turbine entry temperatures. Maintaining adequate life at these temperatures requires the development of materials and efficient cooling methods. One cooling method that has gained increasing importance is endwall film-cooling, where coolant air is discharged through discrete holes in the inner and outer endwalls of a turbine blade passage. After leaving the holes, the coolant air forms a protective layer between the hot mainstream gas and the surface that is to be protected. Several numerical methods are available to solve differential equation of heat conduction, among these methods are the finites volume, finite elements and control volume approaches in many applications the turbine blades have complex geometries, therefore, in the present study a new methods to solve this problem by using the upwind differencing scheme [1]. Also, it is found an effect of end wall coolant ejection on the flow in the blade passage, indicating that coolant ejection may reduce secondary flow [2]. [3] reduced secondary flow in a linear cascade by ejecting air from a slot in the end wall upstream of the leading edge plane. He measured a reduction in secondary losses which unfortunately was more than offset by the energy required for the air ejection. He concluded that a net benefit could be achieved if the ejected air was used for cooling purposes.

Cooling configuration:

To minimize the effect of high temperature of gases passing upon turbine blade, cooling systems are used cool the turbine to reasonable temperature which is not to cause damages to the turbine blade and to enhance the material resistance to the maximum turbine inlet temperature which increases with time . Therefore, gas turbine designers have to seek ways for increasing the turbine inlet temperature at a rate faster than materials will allow. One solution was the use of turbine cooling, which has allowed the turbine designer to increase the turbine inlet temperature while maintaining a constant blade temperature [4]. The air is the main coolant that has been used with turbine blade cooling. The cooling methods used are convection cooling, impingement cooling, film cooling, and transpiration cooling [3].The air flows outward through a series of radial cooling holes, as shown in Figure(1).

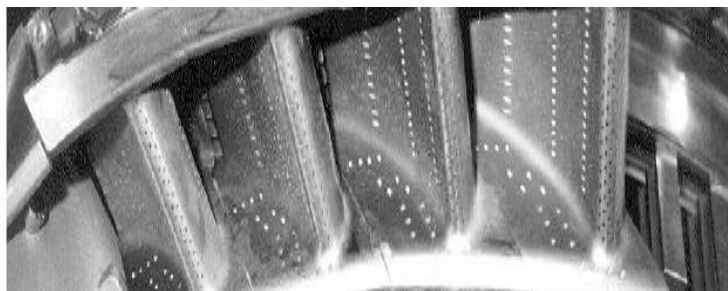


Figure (1) Turbine nozzle guide vane with endwall film cooling ref [3].

The design of the investigated datum of cooling configuration loosely resembles the real engine design shown in fig. (1) ref. [3]. Here, This cooling configuration would provide cooling to most of the endwall surface in the absence of secondary flow. It is therefore well suited to investigate the interactions between the ejected coolant and the endwall flow field [5]. In this research cooling configuration, coolant air is ejected through 25 holes in one endwall of a single passage. fig. (2) shows the cooling configuration that consists of three single rows of holes, all having a diameter of 1 mm and ejecting at an angle of 45° to the surface. The first row of holes is located at 99% axial chord and ejects in approximately the inviscid streamline direction. While The second's row is at 90% axial chord, again ejecting in approximately the inviscid flow direction. The third row of holes is located at 75% axial chord.

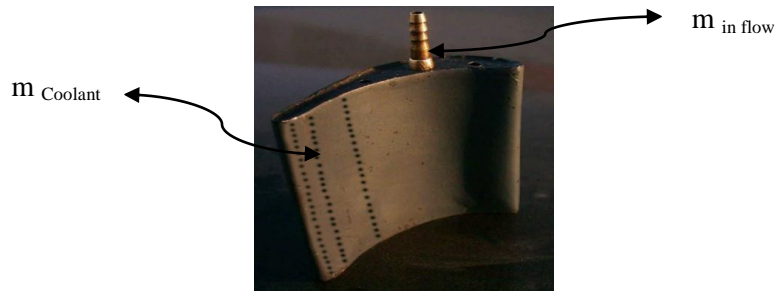


Figure (2) Schematic of the mixing

Mixing Analysis:

The flow within the coolant hole is three-dimensional, as can be seen in the computational predictions of [6]. A separation at the hole inlet is the cause of a pair of counter-rotating vortices and a region of increased velocity opposite of the separation bubble. The blockage created by the jet as it enters the mainstream creates a local variation in pressure at the hole exit. After leaving the hole, the coolant mixes with the mainstream. An approximation of the entropy generated during this mixing process can be obtained by assuming that the mixing takes place within a short distance downstream of the hole, thus justifying a constant static pressure mixing calculation. The mixing calculation is similar in character to the one-dimensional analytical model proposed by [7]. For this mixing calculation, the blade passage is divided into several mixing control volumes in the vicinity of the coolant holes. In the mixing calculation the equations for the conservation of mass, momentum and energy are applied to the mixing control volume. The static pressure is taken to be constant during the mixing process, using the hole exit velocity and temperature.

The outflow values of stagnation pressure and temperature from each of the mixing control volumes are mass averaged to determine the overall stagnation. The mixture laws [8] are: $MR = (C_{coolant}/M_{inflow})$ All the dimensions for this blade cascade can be found in Table (1)

Number of blades		4
Chord	[mm]	67
Pitch	[mm]	100
Span	[mm]	60
T_{hg}	[k°]	350
T_p	[k°]	293
No. holes		25
V_R		0.5, 1 and 2

Table (1) The Dimensions and Angles for Blade Cascade

Test Rig:

A test rig has been designed and constructed in order to investigate the effect of cooling air passage on the temperatures distribution. The temperatures are measured as follows; the surface temperatures are measured by wireless temperatures measurement as in figure [3-a] and temperatures between passages are measured by thermometers types' k/j as shown in figure [3-b]. All the calibration possible has been made to certify the flow parameters in the test rig section can be shown that this made [3]. In the present investigation the cascade forms 4 blades and an aspect ratio of 1.5 is used. The blades are made from Aluminum smooth sheets. The blade section is selected as given in [3][9]. The cascade consists of four isolated blades two of them represent the test rig walls and the other two lies in between them in the working section as a row of blades. The hot air is provided from the exhaust I. C. Engine to the settling chamber (air box) to damp the delivery flow of air as shown in the figure [4].



Figure (3-a) Temperatures Measurement



Figure (3-b) Thermometers Types k/j



Fig (4) A Photo of the Test Rig Layout.

Measurement procedure:

Before starting the reading, two tests are made to check the instrumentation. The first test is to ensure that the pressure reading in micro-manometer is zero before running. After running, the second test is to make sure of there is no leaking in the pressure lines. In this case the five-hole probe is fitted with a cap, which makes sure that the tubes of the probe connected to each other, and hence registers the same pressure. Then, if there is any significant difference between the two readings for any of the pressure, there is a leak in one of the pressure lines. The calibration process for the five hole probe is very sensitive to the probe alignment, probe support, and any blockage so the procedure is repeated many times until getting smoothing curves where the polynomial curve-fit method fourth-order was used. The accuracy of the processed data shown in table (2) which has good accuracy with a range of errors of approximately not exceeded ($\pm 2.5\%$). The measured temperatures on the surface of both sides of the blade are practiced. A measured temperature in the passage theory and that it is difficult to obtain in practice because of the nature of the design of the system. Therefore, it is founds an error rate ranging from 15% to 10% and this is acceptable ratio. Tables (3),(4) represent the head of the measured pressure by manometer at maximum and minimum blowing ratio and tables (5),(6) represent the velocities component in three axes at maximum and minimum blowing ratio , which was calculated on the basis of the pressure measurement see ref [3].

Pitch Angle in deg.			Yaw Angle in deg.			in (m/sec) Velocity		
Actual	Measured	Error %	Actual	Measured	Error %	Actual	Measured	Error %
-20	-19.8	1	-20	-20.4	1.9	15.6	15.9	1.9
-20	-19.7	1.5	0	-0.5	1	15.9	16.1	1.2
-20	-19.9	0.5	20	20.5	2.5	15	14.8	1.3
0	0	0	20	19.4	3	15.7	16.1	2.5
0	-0.1	1	0	-0.3	1	15.1	14.9	1.3
0	0	0	-20	-20.6	3	15.8	16	1.2
+20	19.7	1.5	-20	-20.4	2	15.9	16.3	2.5
+20	19.9	0.5	0	-0.4	1	15	14.7	2
+20	19.6	2	20	-19.5	2.5	15.1	15.4	1.9

Table (2) The Errors in Probe

<i>Axel cored</i>	h_1 (mm)	h_2 (mm)	h_3 (mm)	h_4 (mm)	h_5 (mm)
0.1	58	21	41	19	60
0.2	32	30	16	12	25
0.3	35	26	12	14	28
0.4	60	25	24	10	57
0.5	66	18	25	6	55
0.6	50	14	25	5	60
0.7	53	15	34	8	60
0.8	57	21	41	20	62
0.9	60	26	50	26	61
1	57	29	52	25	55

Table (3) The Head of the Pressure Measured by the Manometer in (mm) at the Blowing Ratio equal 2.

<i>Axel cored</i>	h_1 (mm)	h_2 (mm)	h_3 (mm)	h_4 (mm)	h_5 (mm)
0.1	24	20	19	15	39
0.2	22	20	18	10	30
0.3	25	12	17	4	17
0.4	36	10	16	4	29
0.5	29	9	12	3	34
0.6	28	8	13	2	43
0.7	32	15	23	8	36
0.8	35	15	28	14	35
0.9	36	18	24	13	30
1	38	19	25	12	35

Table (4) The Head of the Pressure Measured by the Manometer in at the Blowing Ratio Equal 0.5.

<i>Axel cored</i>	<i>u (m/s)</i>	<i>v (m/s)</i>	<i>w (m/s)</i>
0.1	20.10604	17.36339	17.21064
0.2	4.487169	-16.45665	-15.16894
0.3	8.806578	-13.4 0265	7.538373
0.4	7.584979	-26.57206	-25.64113
0.5	21.44158	4.292778	-2.863017
0.6	4.032911	28.5851	-25.83213
0.7	.6756414	-28.05618	-4.327707
0.8	3.877046	-25.05417	-24.83376
0.9	7.660995	-16.06971	-6.557761
1	7.675498	22.60313	-17.17133

Table (5) The Velocities Component in Three Axes, at the Blowing Ratio Equal 2.

<i>Axel cored</i>	<i>u (m/s)</i>	<i>v (m/s)</i>	<i>w (m/s)</i>
0.1	9.265227	1.342176	1.237152
0.2	5.311697	-8.083823	4.546778
0.3	16.99755	2.511499	-2.269622
0.4	6.106856	20.48469	-13.66202
0.5	3.965947	-20.10223	13.40694
0.6	16.43545	11.79174	-10.6561
0.7	.8742069	-19.15878	-2.95527
0.8	.475009	-19.72487	-3.04259
0.9	3.25122	17.82363	7.273503
1	16.19796	-11.62135	10.50212

Table (6) Velocities Component in Three Axes, at The Blowing Ratio Equal 0.5.

Mathematical modeling:

Some scientists have recently tackled the turbulent flow problem by attempting to solve the time-dependent Navier-Stokes equations directly using numerical methods. The usual practice is to consider the time-averaged versions of the governing equations. This follows the assumption that the main flow variables such as the velocity components, etc, may be expressed as the sum of a time-averaged mean value and a fluctuating component about this mean value is referred to [10]. Thus the instantaneous value of each variable (Φ) (i.e. $u, v, w, p, t...etc$) is:

$$\Phi = \overline{\Phi} + \Phi' \quad \dots(1)$$

where:

($\overline{\Phi}$) and (Φ') are the time averaged and fluctuating components of the variable respectively. In this formulation, it is assumed that the time average of the fluctuating components is zero.

(i) Continuity.

$$\frac{\partial U}{\partial x} + \frac{\partial V}{\partial y} + \frac{\partial W}{\partial z} = 0 \quad \dots(2)$$

(ii) Momentum.

In x-direction

$$\begin{aligned} \rho[U \frac{\partial U}{\partial x} + V \frac{\partial U}{\partial y} + W \frac{\partial U}{\partial z}] = -\frac{\partial p}{\partial x} + \frac{\partial}{\partial x} [\mu \frac{\partial U}{\partial x} - \overline{\rho u' u'}] + [\frac{\partial}{\partial y} [\mu \frac{\partial U}{\partial y} - \overline{\rho u' v'}] \\ + \frac{\partial}{\partial z} [\mu \frac{\partial U}{\partial z} - \overline{\rho u' w'}] + S_u \end{aligned} \quad \dots(3)$$

In y-direction

$$\begin{aligned} \rho[U \frac{\partial V}{\partial x} + V \frac{\partial V}{\partial y} + W \frac{\partial V}{\partial z}] = -\frac{\partial p}{\partial y} + \frac{\partial}{\partial x} [\mu \frac{\partial V}{\partial x} - \overline{\rho u' v'}] + [\frac{\partial}{\partial y} [\mu \frac{\partial V}{\partial y} - \overline{\rho v' v'}] \\ + \frac{\partial}{\partial z} [\mu \frac{\partial V}{\partial z} - \overline{\rho v' w'}] + S_v \end{aligned} \quad \dots(4)$$

In z-direction

$$\begin{aligned} \rho[U \frac{\partial W}{\partial x} + V \frac{\partial W}{\partial y} + W \frac{\partial W}{\partial z}] = -\frac{\partial p}{\partial z} + \frac{\partial}{\partial x} [\mu \frac{\partial W}{\partial x} - \overline{\rho u' w'}] + [\frac{\partial}{\partial y} [\mu \frac{\partial W}{\partial y} - \overline{\rho v' w'}] \\ + \frac{\partial}{\partial z} [\mu \frac{\partial W}{\partial z} - \overline{\rho w' w'}] + S_w \end{aligned} \quad \dots(5)$$

(iii) Energy.

$$\rho \frac{\partial V_i}{\partial t} + \rho V_j \frac{\partial V_i}{\partial x_j} = -\frac{\partial p}{\partial x_i} + \frac{1}{Re} \frac{\partial^2 V_i}{\partial x_j \partial x_j} \quad \dots(6)$$

$$Re = \frac{\rho \cdot V \cdot L}{\mu} = \frac{V \cdot L}{\nu}$$

$$c_p \rho \frac{DT}{Dt} = \frac{V_s^2}{(T_w - T_s) c_p} \frac{DP}{Dt} + \frac{k_s}{V_s \rho c_p} \nabla^2 T + \frac{\mu V_s}{L \rho c_p} \frac{\phi^*}{(T_w - T_s)}$$

Where $\phi^* = \frac{\phi}{\mu V_s^2 / L^2}$

$$\phi = \mu \left[2 \left(\frac{\partial u}{\partial x} \right)^2 + 2 \left(\frac{\partial v}{\partial y} \right)^2 + 2 \left(\frac{\partial w}{\partial z} \right)^2 + \left(\frac{\partial v}{\partial x} + \frac{\partial u}{\partial y} \right)^2 + \left(\frac{\partial w}{\partial y} + \frac{\partial v}{\partial z} \right)^2 + \left(\frac{\partial u}{\partial z} + \frac{\partial w}{\partial x} \right)^2 \right]$$

But:-

$$\begin{aligned} -\overline{\rho u' u'} &= \mu_t \frac{\partial U}{\partial x} \quad , \quad -\overline{\rho v' v'} = 2 \mu_t \frac{\partial V}{\partial y} \quad , \quad -\overline{\rho u' w'} = \mu_t \frac{\partial U}{\partial z} \\ -\overline{\rho v' w'} &= \mu_t \frac{\partial V}{\partial z} \quad , \quad -\overline{\rho w' w'} = 2 \mu_t \frac{\partial W}{\partial z} \quad , \quad -\overline{\rho u' t'} = \frac{\mu_t}{\sigma_t} \left[\frac{\partial T}{\partial x} \right] \quad \dots(7) \\ -\overline{\rho v' t'} &= \frac{\mu_t}{\sigma_t} \left[\frac{\partial T}{\partial y} \right] \quad , \quad -\overline{\rho w' t'} = \frac{\mu_t}{\sigma_t} \left[\frac{\partial T}{\partial z} \right] \end{aligned}$$

where (σ_t) is the turbulent Prandtl number which includes the eddy thermal diffusivity. When one substitute Eq. (7) in the Reynolds equation (i.e., 2, 3, 4, 5 and 6) the time-averaged equations for continuity, velocity components, temperatures and turbulent variables, take the form:

(i) Continuity

$$\frac{\partial U}{\partial x} + \frac{\partial V}{\partial y} + \frac{\partial W}{\partial z} = 0 \quad \dots(8)$$

(ii) Momentum
In-X direction

$$\rho \frac{\partial}{\partial x} (UU) + \rho \frac{\partial}{\partial y} (UV) + \rho \frac{\partial}{\partial z} (UW) = \frac{\partial}{\partial x} (\mu_{eff} \frac{\partial U}{\partial x}) + \frac{\partial}{\partial y} (\mu_{eff} \frac{\partial U}{\partial y}) + \frac{\partial}{\partial z} (\mu_{eff} \frac{\partial U}{\partial z}) + S_U \quad \dots(9),$$

In-Y direction

$$\rho \frac{\partial}{\partial x} (UV) + \rho \frac{\partial}{\partial y} (VV) + \rho \frac{\partial}{\partial z} (VW) = \frac{\partial}{\partial x} (\mu_{eff} \frac{\partial V}{\partial x}) + \frac{\partial}{\partial y} (\mu_{eff} \frac{\partial V}{\partial y}) + \frac{\partial}{\partial z} (\mu_{eff} \frac{\partial V}{\partial z}) + S_V \quad \dots(10), \text{ and}$$

In-Z direction

$$\rho \frac{\partial}{\partial x} (WU) + \rho \frac{\partial}{\partial y} (WV) + \rho \frac{\partial}{\partial z} (WW) = \frac{\partial}{\partial x} (\mu_{eff} \frac{\partial W}{\partial x}) + \frac{\partial}{\partial y} (\mu_{eff} \frac{\partial W}{\partial y}) + \frac{\partial}{\partial z} (\mu_{eff} \frac{\partial W}{\partial z}) + S_w$$

(iii) Energy. ...(11)

$$c_p \rho \frac{DT}{Dt} = E_c \frac{DP}{Dt} + \frac{1}{R_s P_r} \nabla^2 T + \frac{E_s}{R_s} \Phi^* \quad \dots(12)$$

Where $E_c = \frac{V_s^2}{(T_w - T_s) c_p}$

$$Pr = \frac{\mu c_p}{k}$$

$$\mu_{eff} = \mu + \mu_t \quad \dots(13)$$

(Γ_{eff}) is the effective exchange coefficient for heat defined by:

$$\Gamma_{eff} = \frac{\mu}{\sigma} + \frac{\mu_t}{\sigma_t} \quad \dots(14)$$

The main difficulty in solving these equations concerns the determination of unknown correlation which represents turbulent or "eddy" viscosity (μ_t) which is not a fluid property and varies over the flow domain depending on the turbulence conditions. Therefore, before any solution can be obtained they must be expressed in terms of known or calculated quantities. These expressions are called turbulent models.

Turbulence Model:

The $k - \varepsilon$ model is the more common active model for turbulent fluid flow problems. It is also called the two equations model, where it characterizes the local state of turbulence by two parameters: the turbulent kinetic energy (k) and the rate of its dissipation (ε) [10],[11].the kinematic viscosity is related to these parameters by Kolmogrov-Prandtl expression:

$$\nu_t = C_\mu \frac{k^2}{\varepsilon}$$

Where C_μ is an empirical constant.

This model is chosen for modeling the two geometries according to the semi-empirical transport equations for k and ε as described below.

K- ε Turbulence Models:

The distribution of the eddy viscosity throughout the flow domain must be established in order to calculate the momentum and heat diffusion coefficients for equations (9 to 12). This is the job of the turbulence model. By calculating the μ_f distribution, the turbulence model implicitly establishes the relative strengths of turbulent and molecular diffusion. Launder and Spalding, proposed a modified version of the K- ε model. This version has been the most widely applied, and is commonly referred to as the standard K- ε , model. The eddy viscosity at each grid point is related to values of the turbulence kinetic energy (K) and the dissipation rate of turbulence energy (ε):

$$\mu_t = \frac{C_\mu \cdot \rho \cdot K^2}{\varepsilon} \quad \dots (16)$$

where C_μ : an empirical constant. The turbulent energy is defined by the fluctuating velocities $K = \frac{1}{2} \overline{(u'^2 + v'^2 + w'^2)}$.

The local distribution of k and ε requires the solution of two additional transport equations, which are derived from the Navier-Stokes equation. The k-transport equation is given by:

$$\frac{\partial}{\partial x}(\rho U K) + \frac{\partial}{\partial y}(\rho V K) + \frac{\partial}{\partial z}(\rho W K) = \frac{\partial}{\partial x} \left(\frac{\mu_t}{\sigma_k} \frac{\partial K}{\partial x} \right) + \frac{\partial}{\partial y} \left(\frac{\mu_t}{\sigma_k} \frac{\partial K}{\partial y} \right) + \frac{\partial}{\partial z} \left(\frac{\mu_t}{\sigma_k} \frac{\partial K}{\partial z} \right) + G_k - \rho \varepsilon \quad \dots(17),$$

and

$$G_k = \mu_t \left[2 \left(\left(\frac{\partial U}{\partial x} \right)^2 + \left(\frac{\partial V}{\partial y} \right)^2 + \left(\frac{\partial W}{\partial z} \right)^2 \right) + \left(\frac{\partial U}{\partial y} + \frac{\partial V}{\partial x} \right)^2 + \left(\frac{\partial U}{\partial z} + \frac{\partial W}{\partial x} \right)^2 + \left(\frac{\partial V}{\partial z} + \frac{\partial W}{\partial y} \right)^2 \right] \quad \dots(18)$$

The ε transport equation is given by:

$$\frac{\partial}{\partial x}(\rho U \varepsilon) + \frac{\partial}{\partial y}(\rho V \varepsilon) + \rho \frac{\partial}{\partial z}(\rho W \varepsilon) = \frac{\partial}{\partial x} \left(\frac{\mu_t}{\sigma_k} \frac{\partial \varepsilon}{\partial x} \right) + \frac{\partial}{\partial y} \left(\frac{\mu_t}{\sigma_k} \frac{\partial \varepsilon}{\partial y} \right) + \frac{\partial}{\partial z} \left(\frac{\mu_t}{\sigma_k} \frac{\partial \varepsilon}{\partial z} \right) + (C_1 G_k - C_2 \rho \varepsilon) \frac{\varepsilon}{K} \quad \dots(19)$$

Empiricism is introduced into the model through the five constants (C_1 , C_2 , C_μ , σ_k and σ_ε) which are assigned the values given in Table (3). This constant is recommended by [12].

C_1	C_2	C_μ	σ_k	σ_ε
1.44	1.92	0.09	1.0	1.3

Table (7): Constant of Turbulence Model.

The above set of constants has been applied successfully too for many three-dimensional flows around blades [13].

Boundary Conditions:

All the discretized flow equations derived previously are for the internal domain. It is necessary now to implement them at the boundaries. To do so we introduce three types of boundary conditions that are required for the present work, they are:-

1. Inlet condition.
2. Outlet condition.
3. Solid (wall) boundaries.

1. Inlet Boundary Conditions:

The distribution of all flow variables needs to specify at inlet boundaries. The values of k and ε are approximated based on assumed turbulence intensity T_i . Therefore the approximate values of k and ε for internal flows can be obtained by means of the following simple assumed forms:-

$$k_{in} = \frac{3}{2} (u_{\xi_{in}} T_i)^2 \quad \dots(20)$$

$$\varepsilon_{in} = C_\mu^{3/4} \frac{k^2}{l} \quad \dots(21)$$

$$l = 0.07L \quad \dots(22)$$

$$u_\xi = u_{\xi_{in}} \quad \dots(23)$$

$$u_\eta = 0 \quad \dots(24)$$

$$P = P_{in} \quad \dots(25)$$

Where L characterizes length, C_μ is a universal constant, 0.09; l is the length scale of turbulence [11].

2. Outlet Boundary Conditions:

At an outlet the velocity distribution is decided by what is happening within the domain. For incompressible flow the gradients normal to the outlet surface of all quantities are assumed to be zero[11].

If NI is the total number of nodes in the ξ – direction, the equations are solved for cells up to I (ori) = $NI - 1$. Before the relevant equations are solved the values of the flow variables at the next node (NI), just outside the domain, are determined by extrapolation from the interior on the assumption of zero gradient at the outlet plane.

For the u_η -and scalar equations this implies setting $u_{\eta_{NI,j}} = u_{\eta_{NI-1,j}}$ and $\phi_{NI,j} = \phi_{NI-1,j}$

Special care should be taken in the case of the u_ξ -velocity. Calculation of u_ξ at the outlet plane $i = NI$ by assuming a zero gradient gives

$$u_\xi(NI, J) = u_\xi(NI - 1, J) \quad ..(26)$$

During the iteration cycles of the SIMPLE algorithm there is no guarantee that these velocities will conserve mass over the computational domain as a whole [14]. To ensure that overall continuity is satisfied the total mass flux going out of the domain (M_{out}) is first computed by summing all extrapolated outlet velocities. To make the mass flux out equal to the mass flux (M_{in}) coming into the domain all the outlet velocity components $u_\xi(NI, J)$, are multiplied by the ratio (M_{in}/M_{out}). Thus the outlet plane velocities with the continuity correction are given by

$$u_\xi(NI, J) = u_\xi(NI - 1, J) \times \frac{M_{in}}{M_{out}} \quad(27)$$

These values are subsequently used as the east neighbor velocities in the discretized momentum equations for $u_{\xi_{NI-1,J}}$.

3. Wall Boundary Conditions:

The implementation of wall boundary conditions in turbulent flows starts with the evaluation of

$$y^+ = \frac{\Delta y_p}{\nu} \sqrt{\frac{\tau_w}{\rho}}$$

Where, Δy_p is the distance of the near wall node P to the solid surface. A near-wall flow is taken to be laminar if $y^+ \leq 11.63$. The wall shear stress is assumed to be entirely viscous in origin. If $y^+ > 11.63$ the flow is turbulent and the wall function approach is used. The criterion places the changeover from laminar to turbulent near wall flow in the buffer layer between the linear and log-law regions of a

turbulent wall layer. The exact value of $y^+ = 11.63$ is the intersection of the linear profile and log-law so it is obtained from the solution of

$$u^+ = \frac{1}{\kappa} \ln(Ey^+) \quad \dots(28)$$

In this formula κ is von Karman's constant (0.4187) and E is an integration constant that depends on the roughness of the wall. For smooth walls E has the value of 9.793.

Following the optimum near wall relationships for the Standard($k - \varepsilon$) model from extensive computing trials [14].

- ❖ Momentum equation tangential to wall

$$\text{Wall shear stress} \quad \tau_w = \rho C_\mu^{1/4} K_p^{1/2} u_p / u^+ \quad \dots(29)$$

$$\text{Wall force} \quad F_S = -\tau_w A_{cell} = -\left(\rho C_\mu^{1/4} K_p^{1/2} u_p / u^+ \right) A_{cell} \quad \dots(30)$$

- ❖ Momentum equation normal to wall

Normal velocity = 0

- ❖ Turbulent kinetic energy equation

$$\text{Net } K \text{-source per unit volume} = \left(\tau_w u_p - \rho C_\mu^{3/4} K_p^{2/3} u^+ \right) \Delta V / \Delta y_p \quad \dots(31)$$

- ❖ Dissipation rate equation

Set nodal value

$$\varepsilon_p = C_\mu^{3/4} K_p^{3/2} / (\kappa \Delta y_p) \quad \dots(32)$$

These relationships should be used in conjunction with the universal velocity (u^+) for near wall turbulent flows.

$$u^+ = \frac{1}{\kappa} \ln(Ey^+)$$

In order of their appearance in eqs. ((25)-(28)) variables are treated as follows in their discretised equations:

- ❖ u_ξ -velocity component parallel to the wall.

The link with the wall is supported by setting $A_S = 0$ and the wall force F_S from eq. (28), is introduced into the discretised u_ξ -equation as a source term, so

$$S_p = -\frac{\rho C_\mu^{1/4} K^{1/2}}{u^+} A_{cell} \quad \dots(33)$$

- ❖ k -equation.

The link at the boundary is suppressed; we set $A_S = 0$. in the volume source, the second term contains $K^{1.5}$. This is linearised as $K_p^{*1/2} \cdot K_p$, where K^* is

the K -value at the end of the previous iteration, which yields the following source terms S_p and S_u in the discretised k -equation:

$$S_p = -\frac{\rho C_\mu^{3/4} K_p^{*1/2} u^+}{\Delta y_p} \Delta V \quad \text{and} \quad S_u = \frac{\tau_w u_p}{\Delta y_p} \Delta V$$

...(34)

❖ ε -equation.

In the discretised ε -equation the near wall nodes is fixed to the value given by eq. (30), by means of setting the source terms S_p and S_u as follows:

$$S_p = -10^{30} \quad \text{and} \quad S_u = \frac{C_\mu^{3/4} K_p^{3/2}}{\kappa \Delta y_p} \times 10^{30} \quad \dots(35)$$

Near-Wall Regions: The standard form of the K - ε model presented above is only valid in the fully turbulent regions of a flow. Consequently, a different treatment is required near solid walls, where viscous diffusion dominates turbulent diffusion. The common approach is to use the wall function method. With this, no attempt is made to compute the flow within the laminar and semi-laminar regions of the boundary layer where molecular diffusion is significant, rather, the next-to-wall grid points are placed in the fully turbulent effects. The field variables for these next-to-wall grid points are solved using the procedures described previously, but the simple boundary conditions for wall shear and surface convection are replaced with wall-function [12]:

$$\tau_{wall} = \frac{C_\mu^{1/4} K_p^{1/2} \rho u_p}{\frac{1}{k} \ln\left(\frac{E \rho \Delta x_p C_\mu^{1/4} K_p^{1/2}}{\mu}\right)} \quad \dots(36),$$

and

$$q'_{wall} = \frac{C_\mu^{1/4} K_p^{1/2} \rho c_p (T_p - T_{wall})}{\sigma_t \left[\frac{1}{k} \ln\left(\frac{E \rho \Delta x_p C_\mu^{1/4} K_p^{1/2}}{\mu}\right) + \left(\frac{A}{k}\right)^{1/2} \left(\frac{\sigma_L}{\sigma_t} - 1\right) \left(\frac{\sigma_t}{\sigma_L}\right)^{1/4} \right]} \quad \dots(37)$$

The subscript (p) indicates values at the next-to-wall grid points, and Δx_p is the distance from the wall to the next-to-wall grid points. A and E are constants representing wall roughness while k is VonKarman's constant. Since the turbulent kinetic energy of the next-to-wall grid points appears in the wall functions, the boundary condition coefficients must be updated each solution iteration as the k - ε solution field evolves. In essence, the wall-function method assumes the form of velocity and temperature profiles within the boundary layer. If behavior within the boundary layer deviates from the assumed profiles, errors will be introduced of the many constructs of wall functions that had been developed and applied, Launder and Spading recommend this semi-empirical formulation based on their

experience with fully turbulence flow. It is important to note that the logarithmic profile for forced flow is the foundation of Launder and Spading's wall functions. For this reason [12] wall functions are often referred to as the " log-law" wall-functions.

Conserved property	Φ	Γ_{Φ}	S
Mass (continuity)	1	0	0
Direction-I momentum	u_i	μ_{eff}	$-\frac{\partial p}{\partial x_i} + \frac{\partial p}{\partial x_j} [\mu_{eff} + \frac{\partial u_j}{\partial x_i}] - \rho g_i \beta_1 \theta_1$
Turbulence kinetic energy	K	$\frac{\mu_{eff}}{\sigma_k}$	$G_k + G_B - \rho \epsilon$
Turbulence energy dissipation	ϵ	$\frac{\mu_{eff}}{\sigma_{\epsilon}}$	$\frac{\epsilon}{k} [C_{1c} G_k + G_B] - C_2 \rho \epsilon$

Table (8): Exchange Coefficient and Source Terms of Φ .

Results and discussion:

The results have been discussed and performed to simulate a discrete circle hole film cooling flow between passage. The temperature contour pattern of figures (5-a,b and c) shows the maximum temperature occurs at the test was $Vr.= 0.5$ $T_{in} = 293k^0$ and the jet location is (99%)from axial chord ,it is clear form these figures The temperature decreases gradually from the jets core to the outside boundary. From the other side it is shows the maximum temperature occurs at the trailing edge from the suction side. But at the pressure side the temperature associated with high heat transfer in this region, because the temperature decreases gradually from the jet core. A closer inspection of temperature distribution form turbine blade with circular cooling passages shows that the temperature falls quite rapidly and then increase towards the trailing edge, but this reduction extended over greater length of the blade than that on the pressure side.

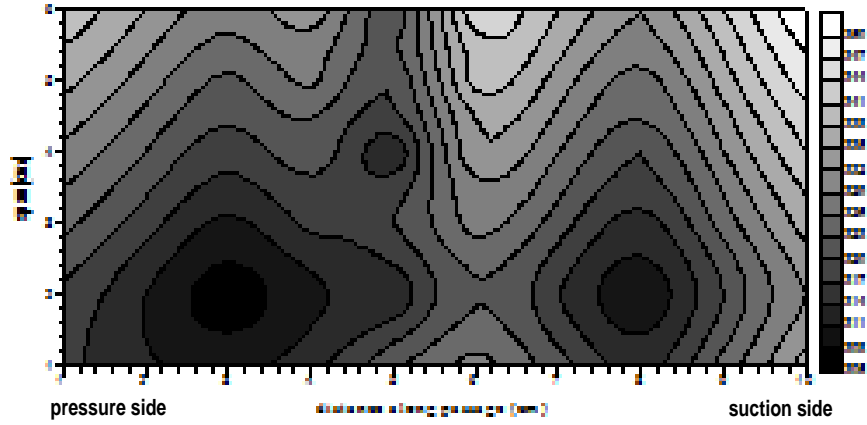
The temperature contour pattern of figures (5-a,b and c) shows the maximum temperature of $(353K^0)$ at the trailing edge from the suction side and at the pressure side the temperature reaches about $(323K^0)$ associated with high heat transfer in this region. Even though large cooling passage is very favorable positioned in this area.

If compared figures [5, 6 and 7] shows the temperature increase with decrease the velocity ratio at the same jet location from the axial chord, due to the flow field appear to be dominated by large numbers of vortexes near the suction surface from the passage, This means that the secondary flow increases with increase in upstream velocity and that it means the velocity ratio are decrease. On the other hand, the mixing losses are reduced with increase velocity ration. From the other side if compared all cases as in figure [8], we notes that the temperature decrease with decrees location of the jets from the axial chord because of the mass flow rate of the jet is high therefore the jets successfully push the vortex out of the passage without impinging on the suction surface and this lead to successfully reducing secondary flow and reducing the temperature. All this causes lead to the temperature increase with decrease in the velocity ratio.

Conclusions:

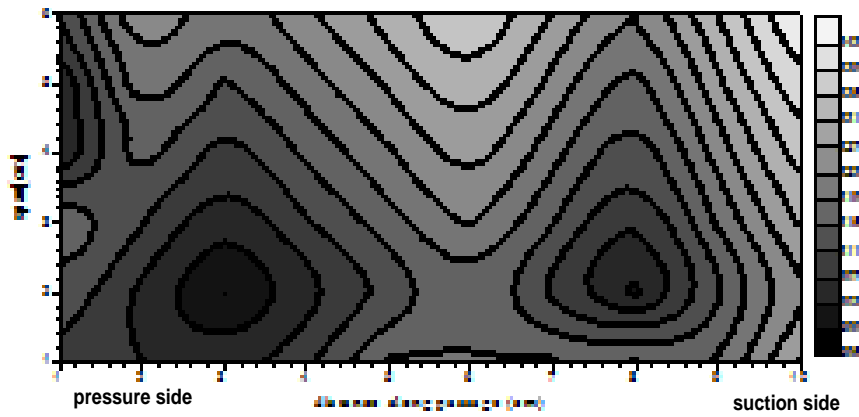
The present work studies the effect of jets location and velocity ration on the temperature distribution in the passage of turbine blades .therefore the present work shows:

- The maximum temperature occurred of $vr = 0.5$ and the jet location (99%).
- The temperature fluctuation decreases gradually from the jet core to the outside.
- Temperatures increase with decrease in the velocity ratio at the same jet location.
- The temperature decreases with decrease at location of the jets at the axial chord



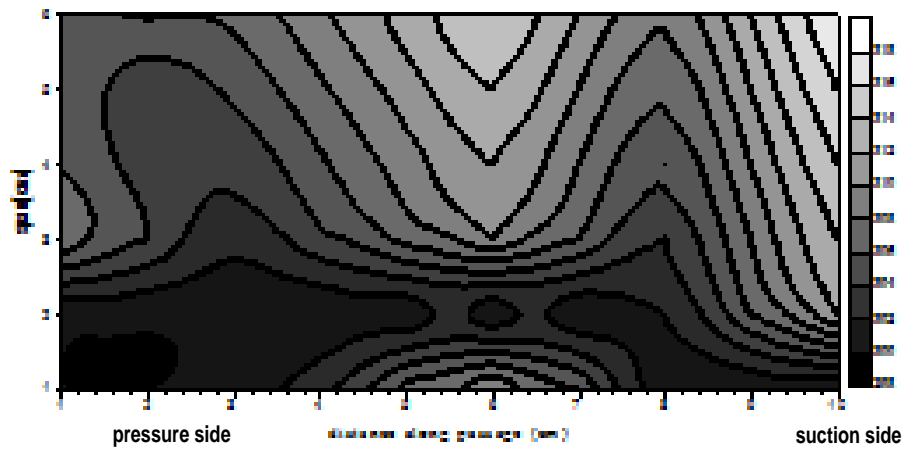
[a]

Figure[5 -a] Temperature variation contour at the blowing ratio[0.5] locale[99%] end wall



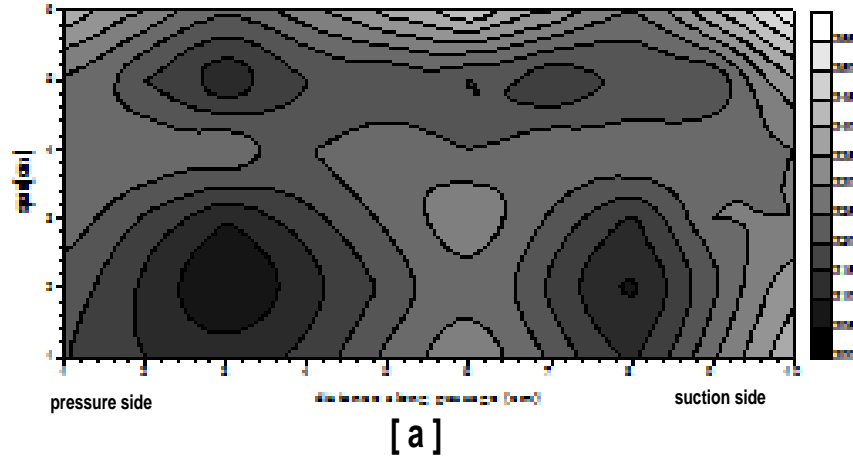
[b]

Figure[5 -b] Temperature variation contour at the blowing ratio[0.5] locale[90%] end wall

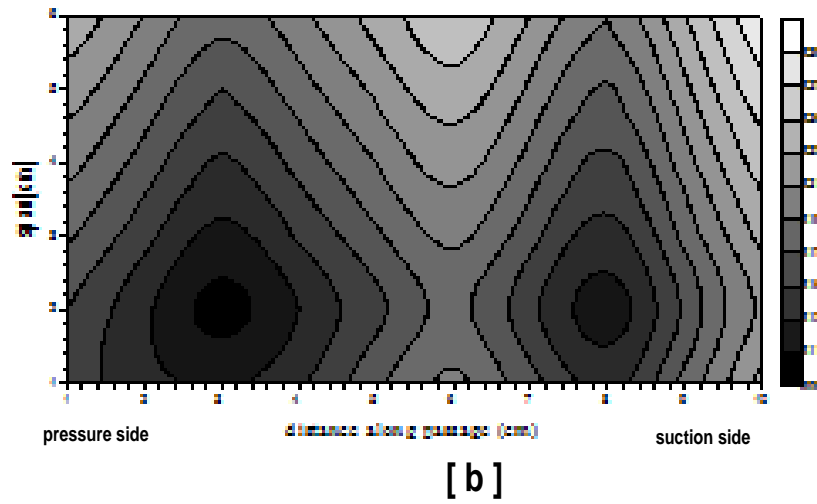


[c]

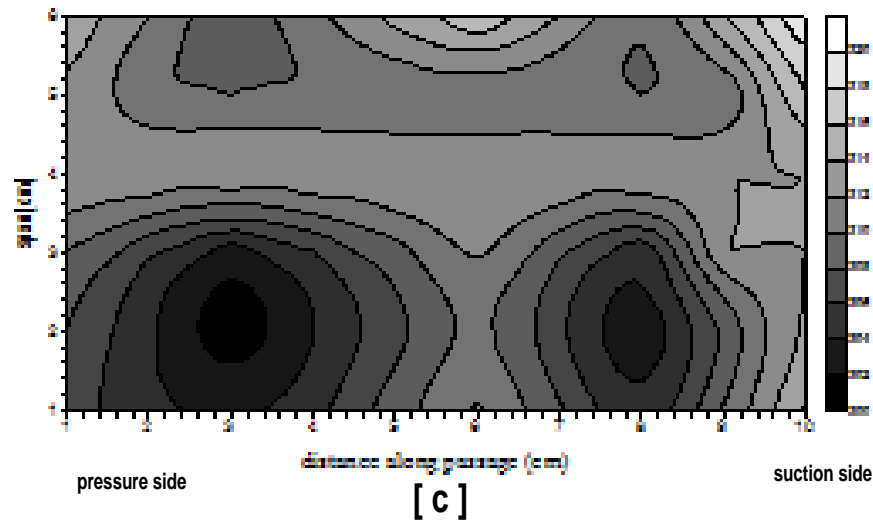
Figure[5 -c] Temperature variation contour at the blowing ratio[0.5] locale[75%] end wall



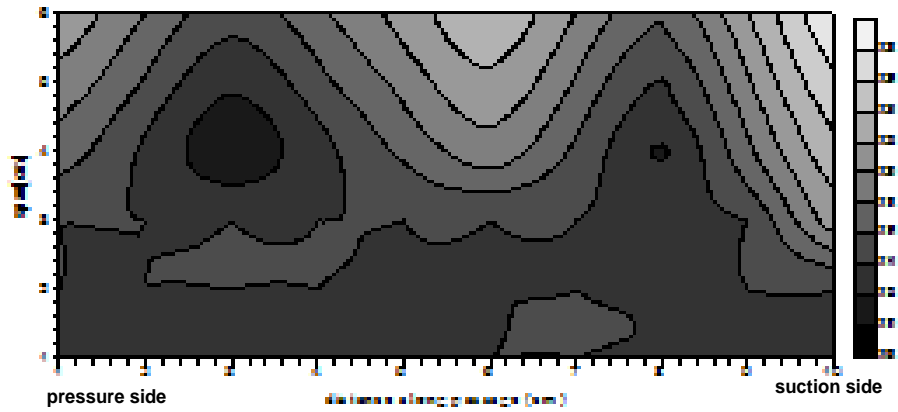
Figure[6 -a] Temperature variation contour at the blowing ratio[1] locale[99%] end wall



Figure[6 -b] Temperature variation contour at the blowing ratio[1] locale[90%] end wall

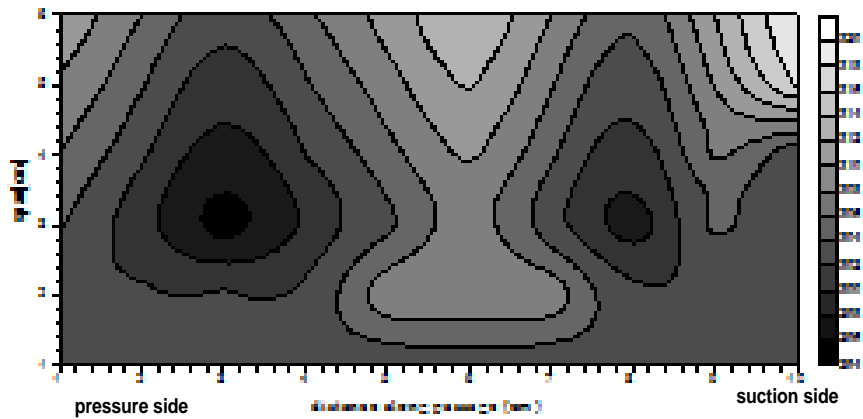


Figure[6 -c] Temperature variation contour at the blowing ratio[1] locale[75%] end wall



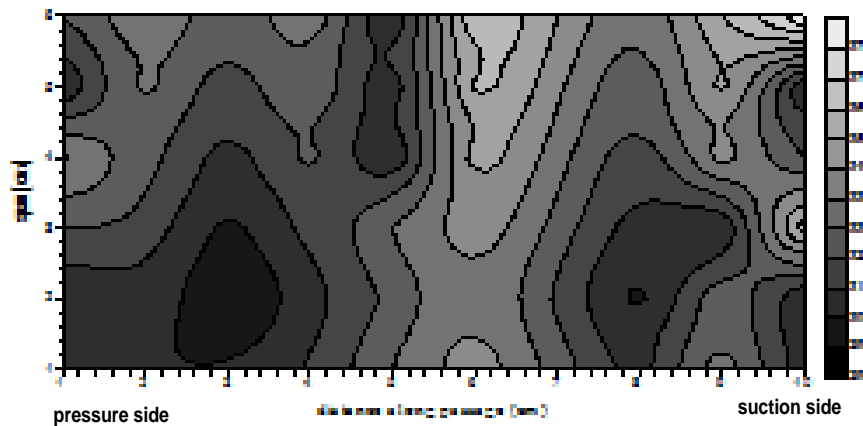
[a]

Figure[7 -a] Temperature variation contour at the blowing ratio[2] locale[99%] end wall



[b]

Figure[7 -b] Temperature variation contour at the blowing ratio[2] locale[90%] end wall



[c]

Figure[7 -c] Temperature variation contour at the blowing ratio[2] locale[75%] end wall

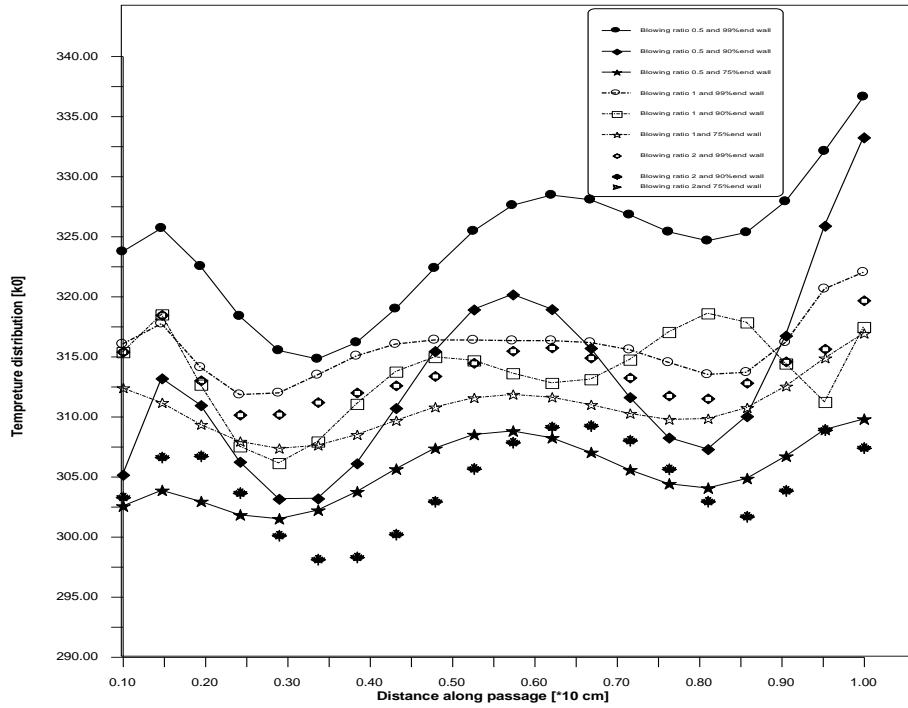


Figure [8] The Temperature Variation at Different Cases

Nomenclatures

$a1, a2, b1$	Coordinate transformation coefficient
aa, bb, cc, dd	Coefficient in the pressure correction equation
A	Combined diffusion-convection coefficient
c_1, c_3	Geometric quantities
$C_\xi, C_\eta, d_\xi, d_\eta$	Coefficients
$C_\mu, C_{\varepsilon 1}, C_{\varepsilon 2}$	Constants in the $k-\varepsilon$ model
D	Diffusion term
E	Constant used in the law of the wall
F	Convection term
G1, G2	Contravariant velocity components
K	Turbulent kinetic energy
L	Characteristics length
P	Pressure
S	Source term
u, v	Cartesian velocity components
u_ξ, u_η	Covariant velocity components
x, y	Cartesian coordinates
y^+	Non-dimensional distance

δ_ξ, δ_η	Distance between two adjacent nodes
Δ_ξ, Δ_η	Distance between control volume faces
ΔV	Volume of control unit
Δy_p	The normal distance from the wall surface to nodal point neighboring to the wall
Γ	Diffusion coefficient
ε	Dissipation rate of turbulent kinetic energy $\sigma_k, \sigma_\varepsilon$
κ	Von karman constant
ξ, η	Curvilinear coordinate
ρ	Density
$\sigma_\kappa, \sigma_\varepsilon$	Constants in the $k - \varepsilon$ model
τ_w	Wall shear stress
ϕ	Dependent variable
ψ	Stream function

Subscripts

e,w,n,s	Faces of control volume
E,W,N,S	Neighbor nodes of point P
in	Inlet
MX,MY	Source term of momentum equation in Cartesian coordinates
u_ξ, u_η	Source term of momentum equation in curvilinear coordinates
nb	Abbreviation of neighboring
out	Outlet
x,y	Partial derivative in the physical plane
ξ, η	Partial derivative in the computational plane
ε	Source term of ε equation
k	Source term of k equation

References:

1. James D., Heidmann, S. and Hunter, D., 2001, "Coarse Grid Modeling of Turbine Film Cooling Flows Using Volumetric Source Terms" NASA/TM—2001-210817.
2. Ken I. T., and Takasago S.A., 2000, "Contribution of Heat Transfer to Turbine Blades and Vanes for High Temperature]
3. Stefan F., 1997 "End wall film cooling in axial turbine "Cambridge university Engineering Department.
4. Javadi1 A., Javadi1 K., Taeibi-Rahni M., and Darbandi M., 2003, " A New Approach to Improve Film Cooling Effectiveness Using Combined Jets" Proceedings of the International Gas Turbine Congress Tokyo November 2-7, 2003IGTC2003Tokyo TS -071.
5. Karcz M., 2003, " Performance Analysis of the Thermal Diffusers—The Gas Turbine Cooling Aspects", PhD Thesis, Institute of Fluid-Flow Machinery PAS, Thermo-Chemical Power Department, Gdańsk.
6. Leylek J. H., and Zerkle R. D., 1993, "Discrete–Jet Film Cooling "ASME paper 93-GT-207.
7. Hartsel, J.E., 1972, "Prediction of Effects of Mass-Transfer Cooling on the Blade-Row Efficiency of Turbine Airfoils", AIAA Paper No. 72-11.
8. Mattingly J.D., Heiser W.H., Daley D.H., 1989, "Aircraft Engine Design", Department of Aerodynamic United States Air Force Academy , Colorado Springs, Colorado.
9. Abuaf N. and Kercher D.M., "Heat Transfer and Turbulance in a Turbulated Blade Cooling Circuit", **Journal of Turbomachinery** ,Vol.116, pp.169-177, 1994.
10. Patankar, S.V., and Spalding, D.B., "A Calculation procedure for heat, mass, and momentum transfer in three-dimensional parabolic flows", J. Heat Mass Transfer, Vol.15, 1972, PP.1787-1806.
11. Dr. H. Yousif (2007) Numerical Investigation of Mixing Losses Downstream of a Turbine Cascade. Mechanical Engineering Industrial Gas Turbines", <http://www.google.com> (Key Words "Turbine Blade Cooling"). [Paper Department,
12. Launder B.E., and Spalding D.B., 1974, "The Numerical Computation of Turbulent Flows", Computer Methods in Applied Mechanics and Engineering, Vol. 3, pp. 269-289.
13. Theodoridis G.S., Lakhel D., and Rodi W., 2001, "Three-Dimensional Calculations of the Flow Field around a Turbine Blade with Film Cooling Injection near the Leading Edge" Institute for Hydromechanics, University of Karlsruhe, Kaiserstrasse 12, D-76128 Karlsruhe, Germany.
14. Versteeg, H. K., and Malalasekera, W., " An introduction to computational fluid dynamics, the finite volume method ", 1995.

Recived (9/6 /2010)

Accepted (24/8/2010)

